Available online at www.sciencedirect.com

SciVerse ScienceDirect

Ceramics International 38 (2012) 3659–3666

CERAMICS INTERNATIONAL

www.elsevier.com/locate/ceramint

Bismuth-catalyzed synthesis of ZnO nanowires and their photoluminescence properties

Han Gil Na, Ju Chan Yang, Dong Sub Kwak, Hyoun Woo Kim *

Division of Materials Science and Engineering, Hanyang University, Seoul 133-791, Republic of Korea

Received 6 September 2011; received in revised form 28 December 2011; accepted 3 January 2012
Available online 27 January 2012

Abstract

By means of heating a mixture of Zn and Bi powders, we have successfully prepared ZnO nanowires. Since the produced nanowires correspond to the pure hexagonal ZnO phase with no catalytic nanoparticles being observed at the tips, the growth is dominated by the base-growth mechanism, in which Bi species at the bottom of the nanowires played a catalytic role. Photoluminescence (PL) analysis of indicated that the integrated intensity ratio of the 2.5 eV-band to the UV band increased with increased growth temperature. An increase of the Bi_2O_3 phase itself, Bi_2O_3 phase-induced oxygen vacancies, and an increase of oxygen vacancies in ZnO with increasing growth temperature were responsible for the intensification and the appearance of the 2.5 eV-band.

Keywords: D. ZnO; Bismuth; Nanowires; Photoluminescence

1. Introduction

In recent years, zinc oxide (ZnO) has been drawing the special attention of scientists and technologists around the world due to its versatile and remarkable physical, optical and electronic properties. ZnO is an n-type II–VI semiconductor material with a wide and direct bandgap energy of 3.37 eV and high exciton binding energy of 60 meV; hence, it has come to be considered a novel material of great importance [1–4].

Since some of the long-standing technical problems that have challenged the bulk/thin film community have been resolved by the introduction of semiconductor nanowires, such nanowires have come to be considered potential low-dimensional materials for use in nanoelectronics and optoelectronics [5–8]. Accordingly, strong research efforts have been focused on the study of ZnO nanowires. In particular, ZnO nanowires show promising potential for application in a variety of areas, including ultraviolet (UV) lasers [6], nanogenerators [9], piezoelectric gated diodes [10], gas sensors [11], UV photodetectors [12], photocatalysts [13], field-effect transistors [14], and highly sensitive UV photoconductors that can be used as optoelectronic switches [15]. Wang et al. fabricated ZnO nanowire arrays for use as negative electrodes for lithium-ion batteries [16]. Chang et al. successfully fabricated high-performance ZnO nanowire field-effect transistors [17]. Furthermore, doped ZnO nanowires exhibited ferromagnetic behavior at room temperature [18].

On the other hand, bismuth oxide (Bi_2O_3) has attracted great attention due to its potential for use in applications in several technological fields, such as oxide-ion conductors, piezo-optic materials, solar cells, gas sensors, and ceramic glass manufacturing [19–23]. ZnO–Bi_2O_3 composite materials are considered to have potential applications in a variety of areas, including photocatalysis, nanovaristers, nano light-emitting diodes, gas sensors [24], transistors [25], and pigments [26]. The introduction of Bi_2O_3 into ZnO samples was found to improve the performance of varisters through the infiltration of molten Bi_2O_3 at high temperature (above 800 °C) [27]. Also, it is expected that the Bi_2O_3/ZnO heterojunction will be used in nanodevices, including gas sensors [28].

Among the techniques for fabrication of ZnO nanowires, the vapor phase method has been regarded as one of the most efficient routes. In most of the vapor phase processes, a variety of catalysts, including Au [29], Cu [30], Ag [31], Fe [31], Ni [31], and ZnO buffer layers without a metal catalyst [32], have been implemented.

* Corresponding author. Tel.: +82 2 2220 0382; fax: +82 2 2220 0289.
E-mail address: hyounwoo@hanyang.ac.kr (H.W. Kim).

0272-8842/$36.00
doi:10.1016/j.ceramint.2012.01.005

For the first time, we have successfully synthesized ZnO nanowires with the catalytic assistance of Bi elements. In this study, a thermal evaporation technique using a mixture of elemental Zn and Bi powders was used. This novel technique significantly lowered the temperature for preparing ZnO nanowires and contributed to the thinning of the nanowires. Although the product was comprised of Bi_2O_3 phase as well as ZnO phase, the ZnO nanowires themselves did not comprise Bi elements; thus, the Bi_2O_3 phase was supposed to reside on the bottom of the nanowires. This would result in ZnO–Bi_2O_3 composite structures and thus create new applications with novel properties.

In addition, systematic investigation was carried out to reveal the effects of growth temperature on the structure, morphology, and photoluminescence (PL) properties. We found that the temperature alters the product morphology and structure and changes the optical properties.

2. Experimental

A mixture of Zn and Bi powders, which were fully mixed with a weight ratio of 1:1, was heated in a vertical tubular furnace. A schematic diagram of the experimental apparatus was previously reported [33]. Source powders and Au-coated Si substrates were placed on the lower and the upper holders, respectively, in the center of a quartz tube. The Au-coated substrates were prepared by sputtering an Au layer (thickness = °3 nm) on Si substrates in an ion sputterer (Emitech, K757X). To investigate the temperature effects, we varied the

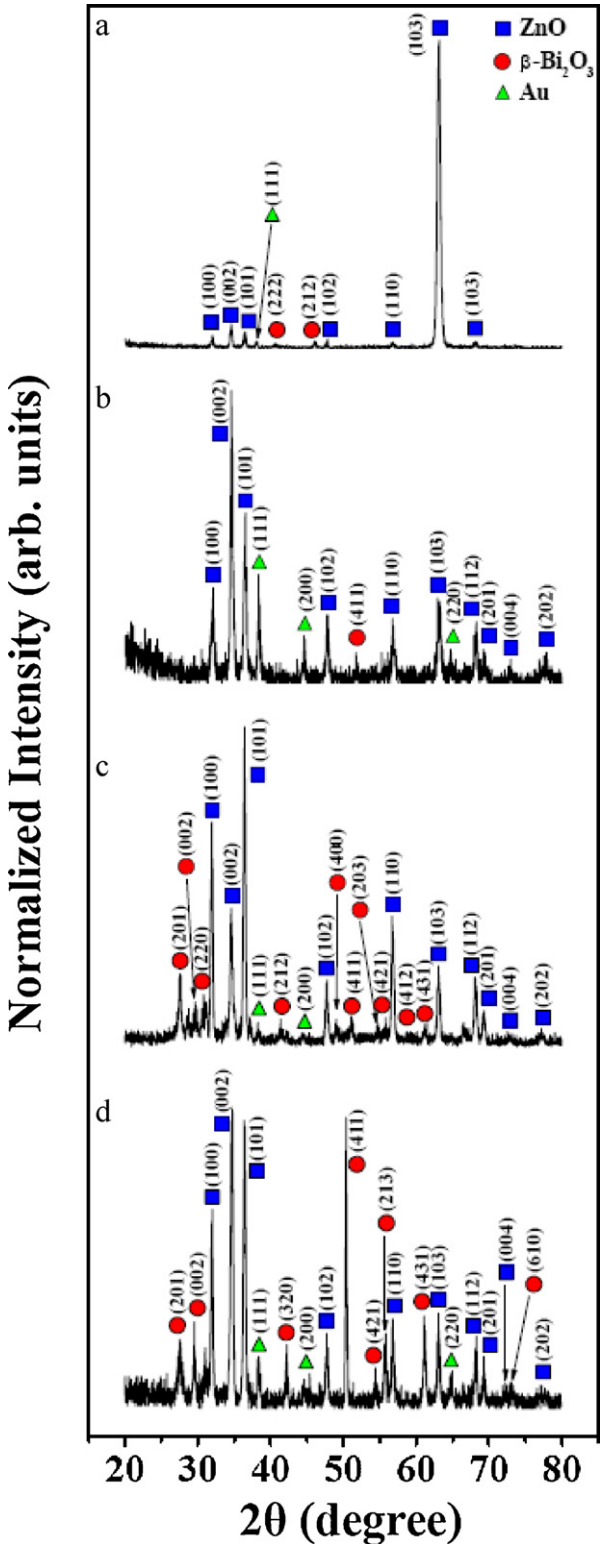

Fig. 1. XRD spectra of products synthesized at (a) 500, (b) 600 °C, (c) 700 °C, and (d) 750 °C.

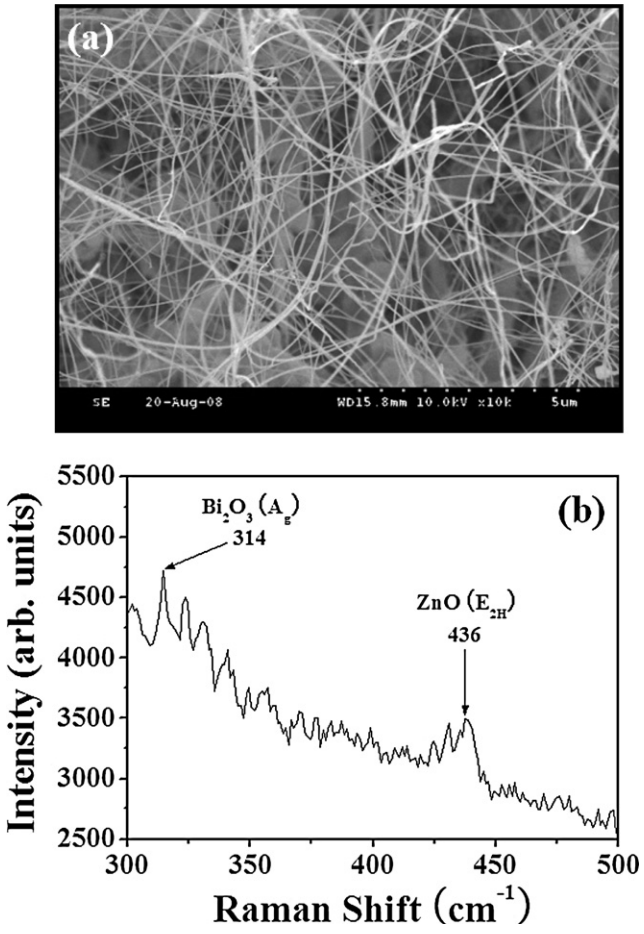

Fig. 2. (a) Top-view SEM image of product synthesized at 750 °C. (b) Corresponding Raman spectrum in the spectral range of 300–500 cm^{-1}.

growth temperature in a range of 500–750 °C. The heating time was set to 1 h, in air ambient.

Scanning electron microscopy (SEM) images were captured using a Hitachi S-4200; glancing angle (0.5°) X-ray diffraction (XRD) patterns were obtained with a Philips X'pert MPD system using Cu $K\alpha_1$ radiation. Transmission electron microscopy (TEM) and energy-dispersive X-ray (EDX) spectra were acquired on a Philips CM 200 operating at 200 kV.

Micro-Raman spectra were obtained using a Renishaw Raman spectromicroscope scanning from 100 cm^{-1} to 1200 cm^{-1} at room temperature in open air. An He–Ne laser beam with a wavelength of 633 nm was used for Raman excitation. PL spectra were measured at room temperature on a SPEC-1403 photoluminescence spectrometer with the 325 nm line from a He–Cd laser (Kimon, Japan).

3. Results and discussion

Fig. 1a–d shows XRD spectra of the products that were synthesized at 500, 600, 700, and 750 °C, respectively. All XRD spectra for the samples grown at 500–750 °C are comprised of diffraction peaks with respect to hexagonal ZnO (JCPDS No. 36-1451) or tetragonal β-Bi_2O_3 (JCPDS No. 27-0050). In addition, there exist reflection peaks of cubic Au from the substrate (JCPDS No. 04-0784). Close examination indicates that the relative intensity of the β-Bi_2O_3-related peaks with respect to the ZnO-related peaks tends to increase with increasing growth temperature. Accordingly, the content of the β-Bi_2O_3 phase is surmised to increase with the increase of the growth temperature.

Fig. 2a shows a SEM image of the product synthesized at 750 °C, revealing that one-dimensional (1D) nanomaterials are densely formed on the substrate surface. Fig. 2b shows the corresponding Raman spectrum, in the spectral range of 300–500 cm^{-1}. The line at 436 cm^{-1} can be assigned to the E_{2H} mode of the ZnO [34]. In addition, the line at 314 cm^{-1} is expected to be due to Bi-O stretch, being ascribed to the tetragonal β-Bi_2O_3 phase [35]. In a previous study, this line was observed in the Raman spectrum of 1D Bi_2O_3 nanohooks [36].

In order to get more structural and morphological information, we have carried out TEM analysis for the samples grown at 750 °C. Fig. 3a shows a low-magnification TEM image of the stem part of the nanowire, revealing that the nanowire possesses straight-line morphology with a relatively smooth surface. Fig. 3b shows a tip part of the nanowires, indicating that no catalytic particles are present at the tip. A typical resolved TEM image taken from the nanowire is shown

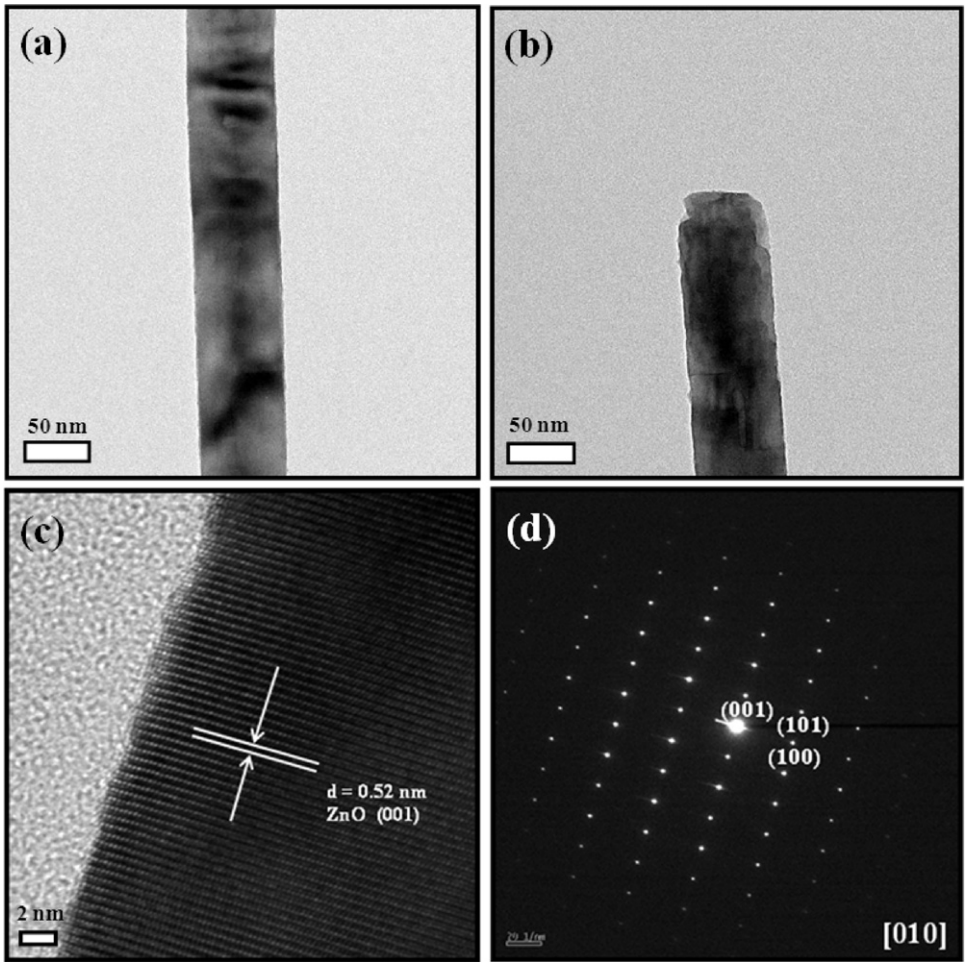

Fig. 3. (a and b) TEM images of 750 °C-grown nanowires. (c) Lattice-resolved TEM image taken near the edge of the nanowires. (d) Corresponding SAED pattern with a [0 1 0] beam direction.

in Fig. 3c. The fringes of the crystalline layers were separated by 0.52 nm, corresponding to the separation between the neighboring {0 0 1} lattice planes of the hexagonal ZnO. Fig. 3d is a corresponding SAED pattern. The single-crystal diffraction spots were indexed as hexagonal ZnO, including (0 0 1), (1 0 1), and (1 0 0) reflections.

We also conducted an EDX analysis with respect to the TEM in order to analyze the composition of the nanowires. Fig. 4a is a low-magnification TEM image of a typical nanowire. Fig. 4b and c shows EDX spectra of the tip and stem parts, respectively, of the nanowire. The EDX analysis reveals that the nanowire is composed of only Zn and O elements, regardless of position, from the stem to the tip. The Cu and C signals are attributed to the carbon-coated Cu grid that supports the nanowire. The arrowheads indicate the position of elemental Bi, revealing that there is no trace of elemental Bi in the ZnO nanowires.

Based on the above observations, we speculated on the growth mechanism of the ZnO nanowires (Fig. 5). Up to the present, there are two well-accepted mechanisms for the growth of nanowires: the vapor–solid–liquid (VLS) and the vapor–solid (VS) mechanisms. Since no Au particles are observed at the tips of the nanowires from the TEM observation, it is not possible to regard the main growth mechanism as the Au-catalyzed tip-growth vapor–solid–liquid (VLS) process. Instead, there may be two possibilities. One is that this type of growth can be ascribed to the VS mechanism, corresponding to a diffusion-limited process in a supersaturated environment. The involved evaporation process can be briefly described as: Zn(s) → Zn(g); Bi(s) → Bi(g). The oxygen source may be the air ambient and residual oxygen in the furnace chamber. In the course of growing nanowires in the axial direction, ZnO and/or Bi_2O_3-related vapors are supposed to adsorb on the nanowire stem surface, resulting in radial growth. However, our EDX and TEM investigations indicate that the ZnO nanowires do not contain elemental Bi, and so we can discard the idea of the VS mechanism (Figs. 3 and 4).

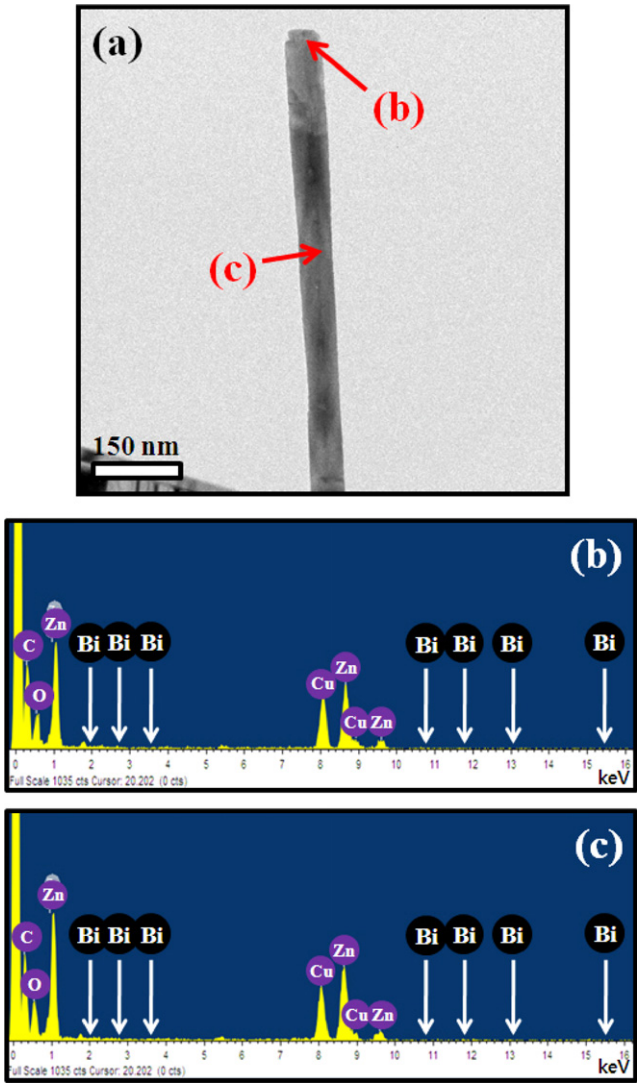

Fig. 4. (a) Typical TEM image and corresponding EDX spectra of the (b) tip and (c) stem part of the nanowire shown in (a). The arrowheads indicate that Bi element is absent.

The other possible explanation is the base-growth VLS mechanism. In this type of VLS process, the liquid droplet may stay at the bottom of the nanowires. Similarly, previous studies on the production of carbon nanotubes [37], MgO nanowires [38], and GeO_2 nanostructures [39] have revealed that such growth could be ascribed to a base-growth mechanism. The vapors may condense into liquid Au–Zn–Bi–O alloy clusters preferentially on the surface of the substrate. Since previous experiments of heating pure Zn powders revealed that Au from the substrate surface played a catalytic role in growing ZnO nanowires, it is likely that the liquid Au–Zn–Bi–O alloy clusters played an important role in the present nanowire growth process. Since no Au was found in the tip region, it is possible that the Au elements on the Si substrate have been dissolved into the alloy droplets on the substrate surface. In addition, the melting temperature of Bi (271.4 °C) is lower than that of Zn (419.6 °C) and thus the addition of Bi will lower the melting temperature of the alloy droplet. It should be noted that Bi has been used as an effective catalyst to grow nanowires via a VLS process [40]. Also, it is well known that Bi_2O_3 has a significantly lower melting point (817 °C) than that of ZnO (1975 °C) [41] and that the ZnO–Bi_2O_3 binary system has a eutectic at 750 °C, giving rise to liquid formation in the sintering process. Accordingly, it is possible that in the present work Bi and/or Bi_2O_3 played a catalytic role in the growth of ZnO nanowires.

In the present base-growth VLS mode, Zn, Bi, and O vapors are continuously incorporated onto the liquid droplets. Once the concentrations of the species become greater than the saturation threshold, ZnO crystals precipitate from the liquid droplets. Accordingly, in the final stage of the synthetic process, the remaining Bi and O elements in the droplet solidify to form Bi_2O_3 (Fig. 5). In addition, ZnO, a typical ionic compound, has a much higher melting point (MP = 1975 °C) than do Zn (MP around 419 °C), Bi (MP around 271 °C), or Bi_2O_3 (MP around 817 °C) [41]. Accordingly, it is reasonable to conclude that oxygen reacted first with Zn to form ZnO. Hence, this can be another reason why ZnO precipitates more readily from droplets containing Bi, Zn, and O than from droplets of the

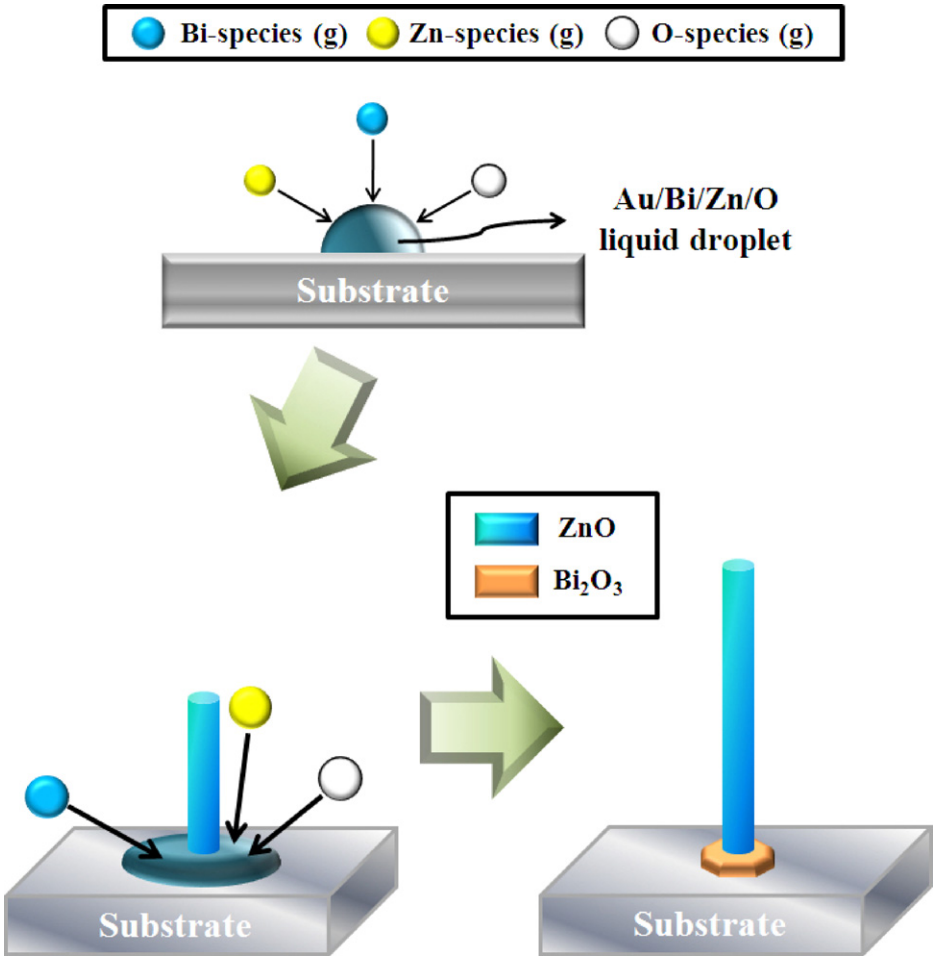

Fig. 5. Schematic illustration of the growth process. In the initial stage, a Zn/Bi/O/Au liquid droplet is formed. In the middle stage, the gaseous Zn-, Bi-, and O-related species are incorporated into the droplet, from which the ZnO nanowires are grown continuously. In the final stage, the remaining Bi and O elements in the droplet solidify to form the Bi_2O_3.

other three materials. Also, at the growth temperature, Zn powder is more inclined to evaporate than Bi powder, resulting in a Zn vapor-abundant ambient. In support of the above argument, the boiling points of Zn and Bi are 907 and 1560 °C, respectively [41]. Of course, under the present conditions, the actual boiling points will be considerably lower than those at the standard conditions. Accordingly, the Zn-abundant nature of the vapors will result in the preferential formation of ZnO nanowires. We surmise that the temperature-induced increase of the vapor pressure of Bi is higher than that of Zn, explaining the gradual increase of content of the Bi_2O_3 phase in the bottom part of ZnO nanowires, with the increase of the growth temperature (Fig. 1).

In the present experiments, the diameter of the produced 1D structures was inclined to decrease with the increase of the growth temperature in the range of 500–600 °C (see Supplementary material S-1). By means of SEM images, we have investigated the morphological changes of products grown at various temperatures in the range 500–750 °C. The products at 600–750 °C exhibited a 1D nanowire morphology with an average diameter in the range 50–52 nm. On the other hand, the 500 °C-grown wires have an average diameter of about 108 nm, which is not in the nanoscale range (see Supplementary material S-2). Accordingly, we have obtained nanowires above 600 °C. Similarly, in our previous study, we synthesized ZnO 1D structures by employing the same method as that in the present work, except that the pure ZnO powders were heated [42]. It is revealed that the morphology was considerably dependent on the growth temperature; the average diameters of 900 °C-, 950 °C-, 1000 °C-, and 1050 °C-grown samples are approximately 379 nm, 140 nm, 100 nm, and 59 nm, respectively. Accordingly, we have obtained nanowires above 1000 °C (see Supplementary material S-3). From the above observations based on the heating of pure or mixed powders, sufficiently high temperature is needed to obtain sufficiently thin 1D nanowires.

It is noteworthy that 1D structures with mixed powders are thinner than those with pure Zn powders at the same temperature. We surmise that the growth of ZnO nanowires by pure Zn powders is mainly controlled by the VS mechanism. In the VS process, the ZnO directly nucleates and grows on the nanowire stem surface, contributing to the thickening of the nanowires. On the other hand, the growth of ZnO nanowires by mixed Zn nanowires is mainly controlled by the base-growth

VLS mechanism, and more adatoms will be diffused to the bottom catalytic droplets, which are energetically favorable sites. Accordingly, it is likely that the nanowires grown by mixed powders will have a smaller diameter than those grown by pure Zn powders.

On the other hand, in case of using a mixture of Zn and Bi powders, it is not clear why high-temperature-heating is favorable for the thin nanowires. However, the diffusion of adatoms on the nanowire surface becomes smooth and faster with the increase of the temperature. Accordingly, at a higher temperature, more adatoms will be diffused to the bottom droplets, which are energetically favorable sites, instead of remaining on the side surfaces of nanowires. Another possibility is that higher temperature enables a faster desorption of the adsorbed species. Since the bottom droplet part is a more energetically stable region than the stem part (in terms of sticking coefficient), the adatoms on the nanowire side surface will be more likely to be detached than those on the bottom. This tendency will contribute to the formation of thinner nanowires.

The normalized PL spectra of products synthesized by the heating of pure Zn powders at 500 °C, 600 °C, and 750 °C are presented in Fig. 6a–c, respectively. For comparison, those synthesized by heating a mixture of Zn and Bi powders at 500 °C, 600 °C, and 750 °C are presented in Fig. 6d–f, respectively. The PL spectra can be convoluted with Gaussian functions centered at 1.6, 2.5, and 3.2–3.3 eV. Also, the UV emission band peaking at an energy of 3.2–3.3 eV corresponds to the near band edge (NBE) emission, being associated with the excitons in ZnO [43,44]. The weak near-infrared emission at 1.6 eV is presumably attributed to the Zn interstitials [45,46]. The green emission at 2.5 eV in pure ZnO is related to singly ionized oxygen vacancies [47,48].

Based on Fig. 6, we estimated the integrated intensity ratio of deep level (2.5 eV) to UV emissions (Table 1 and Fig. 7). For pure ZnO nanowires, the ratio of deep level to UV emission ($I_{2.5\ eV}/I_{UV}$) is relatively small (<0.1) in the temperature range from 500 °C to 600 °C, but it increases up to 0.486 at 750 °C. Accordingly, we surmise that more oxygen vacancies are generated in ZnO at a higher temperature. Also, for Bi_2O_3-embedded ZnO nanowires,

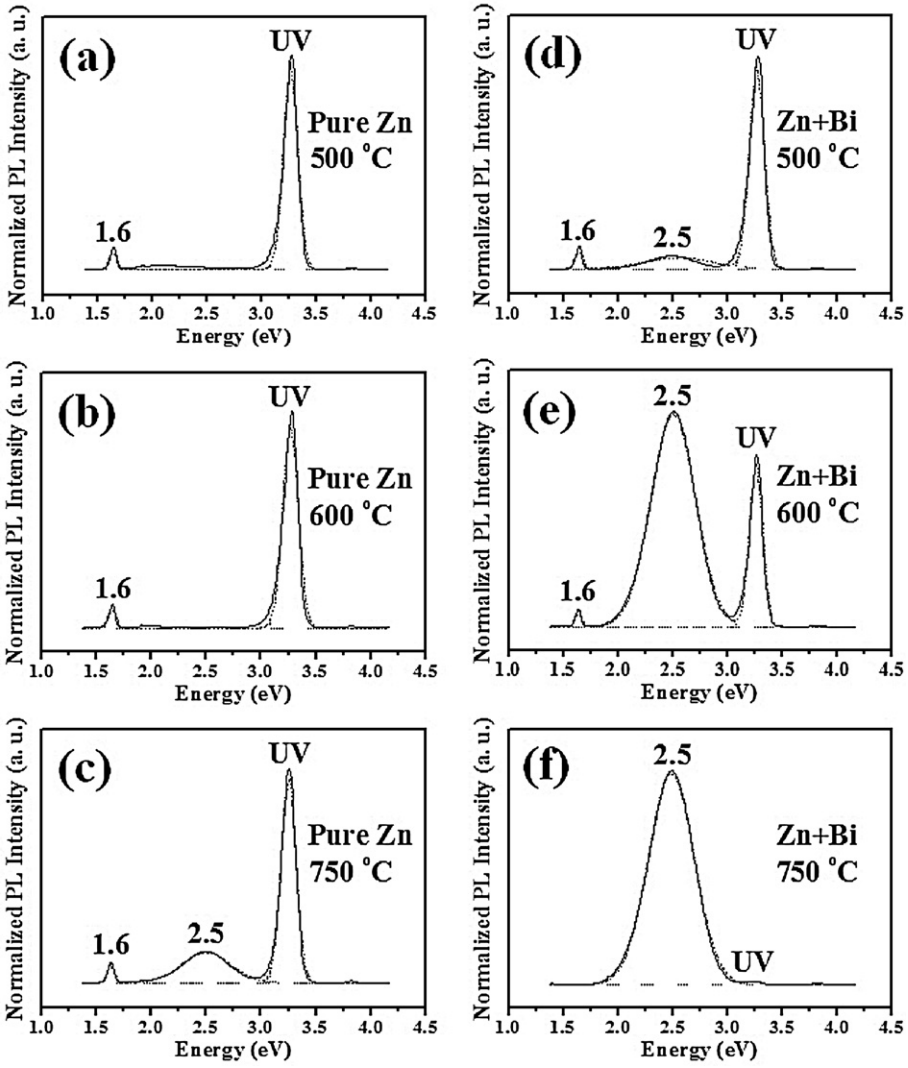

Fig. 6. Normalized PL spectra of the nanowires synthesized by heating (a–c) pure Zn and (d–f) a mixture of Zn and Bi powders at (a and d) 500, (b and e) 600, and (c and f) 750 °C.

Table 1
Integrated intensity ratio of deep level (2.5 eV) to UV emissions with varying the heating temperature for pure ZnO nanowires and Bi_2O_3-embedded ZnO nanowires.

Materials	Integrated intensity ratio ($I_{2.5\ eV}/I_{UV}$)		
	500 °C	600 °C	750 °C
Pure Zn	<0.1	<0.1	0.486
Zn + Bi	0.263	4.395	240.381

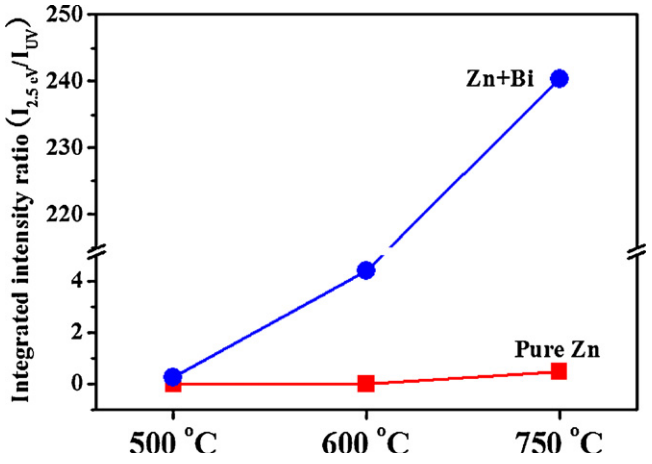

Fig. 7. Variation of integrated intensity ratio of deep level (2.5 eV) to UV emissions with varying the heating temperature. The curves are plotted for the samples which were obtained by heating pure Zn powders and a mixture of Zn and Bi powders, respectively.

$I_{2.5\ eV}/I_{UV}$ increases with increasing the growth temperature. XRD investigation indicates a gradual increase of the Bi_2O_3 phase with increased growth temperature. Because Bi_2O_3 does not exhibit UV emission, the UV band shown in Fig. 6 can be ascribed to ZnO. It is expected that the incorporation of the Bi_2O_3 phase increases the oxygen vacancies (Fig. 7), enhancing the 2.5 eV emission. Furthermore, comparison study reveals that the ratio ($I_{2.5\ eV}/I_{UV}$) of the composite nanowires is larger than that of the pure nanowires, regardless of the heating temperature. In Bi_2O_3–ZnO composite nanostructures, it is known that the incorporation of Bi_2O_3 into ZnO produces more oxygen vacancies due to the generation of the n-type depletion layer at the interface between ZnO and Bi_2O_3 [49]. In addition, it is possible that the green emission arises from the Bi_2O_3 phase in ZnO/Bi_2O_3 nanostructures [25]. The green emission of Bi_2O_3 is associated with the interionic transition of Bi^{3+} ions [50–52]. Furthermore, by increasing the growth temperature in heating the mixture of Zn and Bi powders, the oxygen vacancies in ZnO itself are increased, contributing to the enhancement of 2.5 eV emission.

4. Conclusion

In summary, we heated a mixture of Zn and Bi powders at various temperatures and successfully grew thin ZnO nanowires. XRD and Raman spectra indicate that the products consist of ZnO and Bi_2O_3 phases. The observation of individual nanowires by means of TEM reveals that the nanowires themselves are comprised of pure ZnO phase, with no trace of Bi_2O_3 phase. Since no catalytic nanoparticles were observed at the tips, and because Bi_2O_3 phase was not found in the ZnO nanowire stems, we conclude that the growth of nanowires is dominated by the base-growth mechanism, in which Bi and Bi_2O_3 at the bottom of the nanowires play a catalytic role. The nanowires grown with mixed powders have a smaller diameter than those grown with pure Zn powders, presumably due to the operation of the base-growth mechanism. The thickening of the nanowires at the low temperature of 500 °C can be explained by the reduced diffusion of the adsorbed species. Peak convolution reveals that the PL spectra are comprised of emission bands centered at 1.6, 2.5, and 3.2–3.3 eV. The UV band primarily comes from ZnO, whereas the 2.5 eV band is attributed to oxygen vacancies originating from both the ZnO phase itself and from the incorporation of Bi_2O_3 phase. We suggest that the temperature-induced intensification of the 2.5 eV band is due to an increase of Bi_2O_3 phase itself and/or an increase of oxygen vacancies.

Acknowledgments

This research was supported by Basic Science Research Program through the National Research Foundation of Korea (NRF) funded by the Ministry of Education, Science and Technology (2011-0009946).

Appendix A. Supplementary data

Supplementary data associated with this article can be found, in the online version, at doi:10.1016/j.ceramint.2012.01.005.

References

[1] J. Hupkes, B. Rech, S. Calnan, O. Kluth, U. Zastrow, H. Siekmann, M. Wuttig, Material study on reactively sputtered zinc oxide for thin film silicon solar cells, Thin Solid Films 502 (2006) 286–291.
[2] C.Y. Lee, S.Y. Li, P. Lin, T.Y. Tseng, Field-emission triode of low-temperature synthesized ZnO nanowires, IEEE Trans. Nanotechnol. 5 (2006) 216–219.
[3] S.Y. Li, P. Lin, C.Y. Lee, T.Y. Tseng, Field emission and photofluorescent characteristics of zinc oxide nanowires synthesized by a metal catalyzed vapor–liquid–solid process, J. Appl. Phys. 95 (2004) 3711–3716.
[4] S.N. Bai, T.Y. Tseng, Effect of alumina doping on structural, electrical, and optical properties of sputtered ZnO thin films, Thin Solid Films 515 (2006) 872–875.
[5] P. Yang, R. Yan, M. Fardy, Semiconductor nanowire: what's next? Nano Lett. 10 (2010) 1529–1536.
[6] M.H. Huang, S. Mao, H. Feick, H.Q. Yan, Y.Y. Wu, H. Kind, E. Weber, R. Russo, P.D. Yang, Room-temperature ultraviolet nanowire nanolasers, Science 292 (2001) 1897–1899.
[7] Z.R. Dai, Z.W. Pan, Z.L. Wang, Novel nanostructures of functional oxides synthesized by thermal evaporation, Adv. Funct. Mater. 13 (2003) 9–24.
[8] A.M. Morales, C.M. Lieber, A laser ablation method for the synthesis of crystalline semiconductor nanowires, Science 279 (1998) 208–211.
[9] Z. Wang, J. Song, Piezoelectric nanogenerators based on zinc oxide nanowire arrays, Science 312 (2006) 242–246.
[10] H. He Jr., C.L. Hsin, J. Liu, L.J. Chen, Z.L. Wang, Piezoelectric gated diode of a single ZnO nanowire, Adv. Mater. 19 (2007) 781–784.

[11] H.-W. Ra, K.-S. Choi, J.-H. Kim, Y.-B. Hahn, Y.-H. Im, Fabrication of ZnO nanowires using nanoscale spacer lithography for gas sensors, Small 4 (2008) 1105–1109.
[12] A. Bera, D. Basak, Pd-nanoparticle-decorated ZnO nanowires: ultraviolet photosensitivity and photoluminescence properties, Nanotechnology 22 (2011) 265501.
[13] C. Wu, L. Shen, Y.-C. Zhang, Q. Huang, Synthesis of AgBr/ZnO nanocomposite with visible light-driven photocatalytic activity, Mater. Lett. 65 (2011) 1794–1796.
[14] V.P. Verma, H. Jeon, S. Hwang, M. Jeon, W. Choi, Enhanced electrical conductance of ZnO nanowire FET by nondestructive surface cleaning, IEEE Trans. Nanotechnol. 7 (2008) 782–786.
[15] H. Kind, H. Yan, B. Messer, M. Law, P. Yang, Nanowire ultraviolet photodetectors and optical switches, Adv. Mater. 14 (2002) 158–160.
[16] H. Wang, Q. Pan, Y. Cheng, J. Zhao, G. Yin, Evaluation of ZnO nanorod arrays with dandelion-like morphology as negative electrodes for lithium-ion batteries, Electrochim. Acta 54 (2009) 2851–2855.
[17] P.-C. Chang, Z. Fan, C.-J. Chien, D. Stichtenoth, C. Ronning, J.G. Lu, High-performance ZnO nanowire field effect transistors, Appl. Phys. Lett. 89 (2006) 133113.
[18] C. Xu, J. Chun, D. Kim, B. Chon, T. Joo, Structural characterization and low temperature growth of ferromagnetic Bi–Cu codoped ZnO bicrystal nanowires, Appl. Phys. Lett. 91 (2007) 153104.
[19] M. Yashima, D. Ishimura, Crystal structure and disorder of the fast oxide-ion conductor cubic Bi_2O_3, Chem. Phys. Lett. 378 (2003) 395–399.
[20] A. Feldman, W.S. Brower Jr., D. Horowitz, Optical activity and Faraday rotation in bismuth oxide compounds, Appl. Phys. Lett. 16 (1970) 201.
[21] E.Y. Wang, K.A. Pandelisev, Effect of chemical surface treatments on nonnative (Bi/sub 2/O/sub 3/) GaAs metal–insulator–semiconductor solar cells, J. Appl. Phys. 52 (1981) 4818–4820.
[22] Z.N. Adamian, H.V. Abovian, V.M. Aroutiounian, Smoke sensor on the base of Bi_2O_3 sesquioxide, Sens. Actuators B 35 (1996) 241–243.
[23] A. Pan, A. Ghosh, New family of lead-bismuthate glass with a large transmitting window, J. Non-Cryst. Solids 271 (2000) 157–161.
[24] B.L. Zhu, C.S. Xie, D.W. Zeng, A.H. Wang, W.L. Song, Structure and gas-sensitive properties of ZnO–Bi_2O_3 mixed thick films, J. Inorg. Mater. 20 (2005) 706–712.
[25] B. Ling, X.W. Sun, Y.Q. Shen, Z.L. Dong, Hierarchical ZnO/Bi_2O_3 nanostructures: synthesis, characterization, and electron-beam modification, Appl. Phys. A 98 (2010) 91–96.
[26] P. Sulcova, M. Trojan, Thermal synthesis of the ZnO–Bi_2O_3 pigments, J. Therm. Anal. Calorim. 60 (2000) 209–213.
[27] K. Yuan, G. Li, L. Zheng, L. Cheng, L. Meng, Z. Yao, Q. Yin, Improvement in electrical stability of ZnO varistors by infiltration of molten Bi_2O_3, J. Alloys Compd. 503 (2010) 507–513.
[28] S. Mridha, D. Basak, Investigation of a p-CuO/n-CuO thin film heterojunction for H_2 gas-sensor applications, Semicond. Sci. Technol. 21 (2006) 928–932.
[29] H.J. Yuan, S.S. Xie, D.F. Liu, X.Q. Yan, Z.P. Zhou, L.J. Ci, J.X. Wang, Y. Gao, L. Song, L.F. Liu, W.Y. Zhou, G. Wang, Characterization of zinc oxide crystal nanowires grown by the thermal evaporation of ZnS powders, Chem. Phys. Lett. 371 (2003) 337–341.
[30] K. Yamamoto, K. Nagasawa, T. Ohmori, Preparation and characterization of ZnO nanowires, Physica E 24 (2004) 129–132.
[31] Z. Zhu, T.-L. Chen, Y. Gu, J. Warren, R.M. Osgood Jr., Zinc oxide nanowires grown by vapor-phase transport using selected metal catalysts: a comparative study, Chem. Mater. 17 (2005) 4227–4234.
[32] R.M.B. Cross, M.M. De Souza, E.M. Sankara Narayanan, A low temperature combination method for the production of ZnO nanowires, Nanotechnology 16 (2005) 2188–2192.
[33] H.W. Kim, N.H. Kim, Growth of β-Ga_2O_3 nanobelts on Ir-coated substrates, Appl. Phys. A 80 (2005) 537–540.
[34] J.D. Ye, S.L. Gu, S.M. Zhu, S.M. Liu, Y.D. Zheng, R. Zhang, Y. Shi, Q. Chen, H.Q. Yu, Y.D. Ye, Raman study of lattice dynamic behaviors in phosphorus-doped ZnO films, Appl. Phys. Lett. 88 (2006) 101905.
[35] F.D. Hardcastle, I.E. Wachs, The molecular structure of bismuth oxide by Raman spectroscopy, J. Solid State Chem. 97 (1992) 319–328.
[36] L. Kumari, J.-H. Lin, Y.-R. Ma, One-dimensional Bi_2O_3 nanohooks: synthesis, characterization and optical properties, J. Phys.: Condens. Matter 19 (2007) 406204.
[37] S. Fan, M.G. Chapline, N.R. Franklin, T.W. Tombler, A.M. Cassell, H. Dai, Self-oriented regular arrays of carbon nanotubes and their field emission properties, Science 283 (1999) 512–514.
[38] H.W. Kim, S.H. Shim, Growth of MgO nanowires assisted by the annealing treatment of Au-coated substrates, Chem. Phys. Lett. 422 (2006) 165–169.
[39] H.W. Kim, J.W. Lee, GeO_2 nanostructures fabricated by heating of Ge powders: Pt-catalyzed growth, structure, and photoluminescence, Physica E 40 (2008) 2499–2503.
[40] H.W Kim, S.H. Shim, J.W. Lee, J.Y. park, S.S. Kim, $Bi_2Sn_2O_7$ nanoparticles attached to SnO_2 nanowires and used as catalysts, Chem. Phys. Lett. 456 (2008) 193–197.
[41] I. Barin, Thermochemical Data of Pure Substances, 3rd ed., VCH, Weinheim, Germany, 1995.
[42] H.W. Kim, M.A. Kebede, H.S. Kim, B. Srinivasa, D.Y. Kim, J.Y. Park, S.S. Kim, Effect of growth temperature on the ZnO nanowires prepared by thermal heating of Zn powders, Curr. Appl. Phys. 10 (2010) 52–56.
[43] D.C. Reynolds, D.C. Look, B. Jogai, C.W. Litton, T.C. Collins, W. Harsch, G. Cantwell, Neutral-donor-bound-exciton complexes in ZnO crystals, Phys. Rev. B 57 (1998) 12151–12155.
[44] S.W. Jung, W.I. Park, H.D. Cheong, G.-C. Yi, H.M. Jang, S. Hong, T.S. Joo, Time-resolved and time-integrated photoluminescence in ZnO epilayers grown on Al_2O_3(0 0 0 1) by metalorganic vapor phase epitaxy, Appl. Phys. Lett. 80 (2002) 1924–1926.
[45] R.B.M. Cross, M.M. De Souza, E.M.S. Narayanan, Nanotechnology 16 (2005) 2188.
[46] M. Koyano, P. Quocbao, L.T. Thanhbinh, L. Hongha, N. Ngoclong, S. Katayama, Phys. Status Solidi (a) 193 (2002) 125.
[47] Y. Li, G.W. Meng, L.D. Zhang, F. Phillipp, Ordered semiconductor ZnO nanowire arrays and their photoluminescence properties, Appl. Phys. Lett. 76 (2000) 2011–2013.
[48] O.D. Jayakumar, V. Sudarsan, C. Sudakar, R. Naik, R.K. Vatsa, A.K. Tyagi, Green emission from ZnO nanorods: role of defects and morphology, Scripta Mater. 62 (2010) 662–665.
[49] C. Xu, K. Rho, J. Chun, D.E. Kim, Fabrication and photoluminescence of ZnO hierarchical nanostructures containing Bi_2O_3, Nanotechnology 17 (2006) 60–64.
[50] L. Kumari, J.-H. Lin, Y.-R. Ma, Synthesis of bismuth oxide nanostructures by an oxidative metal vapour phase deposition technique, Nanotechnology 18 (2007) 295605.
[51] A.M. Srivastava, W.W. Beers, On the impurity trapped exciton luminescence in $La_2Zr_2O_7$:Bi^{3+}, J. Lumin. 81 (1999) 293–300.
[52] O.M. Bordun, Luminescence of bismuth-activated ceramics of yttrium and scandium oxides, J. Appl. Spectrosc. 69 (2002) 67–71.